Electronic Supplementary Material (ESI) for Journal of Materials Chemistry C.
This journal is © The Royal Society of Chemistry 2018

# Liquid-Ammonia Synthesis of Microporous $Mg_3N_2$ Showing Intense Red-Light Emission

Viktor Rein[a], Olivia Wenzel[b], Radian Popescu[b], Dagmar Gerthsen[b]*, Claus Feldmann[a]*

a Institut für Anorganische Chemie, Karlsruhe Institute of Technology (KIT), Engesserstrasse 15, D-76131 Karlsruhe (Germany)

b Laboratorium für Elektronenmikroskopie, Karlsruhe Institute of Technology (KIT), Engesserstraße 7, D-76131 Karlsruhe (Germany)

# – SUPPORTING INFORMATION –

**Content**

## 1. Analytical techniques

**Electron microscopy and electron spectroscopy.** Different electron microscopic and electron spectroscopic techniques were applied to study the structural and chemical properties of the obtained nitrides. Overview secondary-electron images were obtained in a ZEISS SUPRA scanning electron microscope (SEM) equipped with a Schottky field emitter at an acceleration voltage of 20 kV and a working distance of 3 mm.

For transmission electron microscopy sample preparation, diluted suspensions of the as-prepared nitrides in chloroform were deposited on silicon wafers and evaporated on a commercial 400 μm mesh Cu-grid (Plano 01824) covered by a holey amorphous carbon film with a nominal thickness of 3 nm. It is noted that the as-received Lacey carbon films contain $SiO_2$ as contamination.

The crystalline structure of $Mg_3N_2$ samples was analyzed by selected area electron diffraction (SAED) in a Philips CM 200 FEG/ST transmission electron microscope at 200 keV electron energy. Transmission electron microscopy (TEM), high-resolution transmission electron microscopy (HRTEM) and high-angle annular dark-field scanning transmission electron microscopy (HAADF-STEM) were performed with an aberration-corrected FEI Titan$^3$ 80-300 microscope at 300 keV.

Energy dispersive X-ray spectroscopy (EDXS) was applied for chemical analysis. EDXS is performed with an FEI Osiris ChemiSTEM microscope at 200 keV electron energy by using a Bruker Quantax XFlash detector. Quantification of the EDXS spectra was carried out with the FEI software package "TEM imaging and analysis" (TIA) version 4.7. Using TIA, element concentrations were calculated on the basis of a refined Kramers' law model, which includes corrections for detector absorption and background subtraction. Standard-less quantification, i.e., by means of theoretical sensitivity factors, without thickness correction was applied. EDXS spectra were obtained during scanning of a rectangular area within a particle ensemble and are used to determine the average chemical composition of the scanned region. The quantification of EDXS area scans is performed on the basis of the characteristic X-ray lines of N (N-$K_{\alpha 1}$) and Mg (Mg-$K_{\alpha}$). We note that X-ray lines of carbon (C-$K_{\alpha 1}$ line) from the amorphous carbon substrate, Cu (Cu-K and Cu-L series) from the grid, as well as, O, Si and F from substrate contamination are observed in all EDXS spectra.

Regarding the O quantification we point out, that the O concentration measured from EDXS area scans on particle ensembles is a sum of the real O concentration within particles and the O contamination on the substrate under the particles. To obtain the real O concentration of the particles, the O concentration on the substrate has to be determined and subtracted from the total measured O content. For that reason, EDXS area scans were separately recorded and quantified on the bare substrate in regions near to the investigated particle ensemble.

Electron energy loss spectroscopy (EELS) was performed with a post-column Tridiem 865 HR Gatan imaging filter (GIF). The energy resolution of about 0.5 eV facilitates fine structure analyses of ionization edges (ELNES: electron energy-loss near edge structure) in EELS spectra, which yield information on the bond characteristics. Specifically, the ELNES of the O-*K*- and the N-*K*-edges was analyzed to distinguish metal oxides and metal nitrides. EELS was performed in the STEM mode.

As a reference as-received, commercial Lacey carbon film copper grids (Ultrathin C Film on Holey Carbon Support Film, 400 mesh, Cu Plano) were characterized by EELS (Figure S1). In addition to the expected carbon (Lacey carbon film), oxygen was observed in certain quantities as indicated by clear absorption peaks. Obviously, this impurity originates from the production process of the Lacey carbon film copper grids. It is important to note that these impurities are independent of the nitride samples.

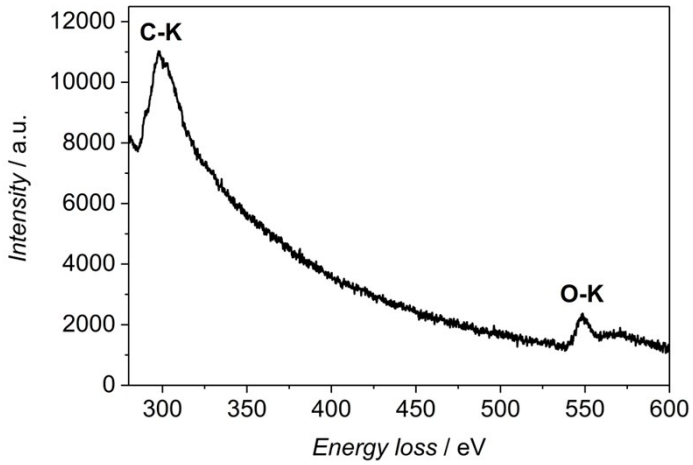


**Figure S1.** EEL spectra of raw Lacey carbon film copper grid showing the presence of C and O as impurities.

**X-ray powder diffraction** was carried out with a Stoe STADI-MP diffractometer by using Cu-$K_{\alpha 1}$ radiation ($\lambda = 1.540598$ Å) monochromated by a focusing Ge crystal. A position sensitive detector (Stoe IP-PSD, 90 °(2θ) angular aperture) was used to record the XRD patterns with a step size of 0.03 °(2θ). The detector channels are calibrated with the line positions of a Si standard. $Mg_3N_2$ powder samples were prepared in glass capillaries under argon for measurement.

**Elemental analysis (C/H/N analysis)** was performed via thermal combustion of $Mg_3N_2$ samples with an Elementar Vario Microcube device (Elementar, Germany) at a temperature of about 1100 °C.

**Fourier-transformed infrared (FTIR) spectra** were recorded with a Bruker Vertex 70 FT-IR spectrometer (Bruker, Germany) in the range 4000-370 $cm^{-1}$ with a resolution of 4 $cm^{-1}$. To this concern, 1 mg of dried $Mg_3N_2$ was pestled with 300 mg of KBr, pressed to a pellet, and measured in transmission geometry.

**Volumetric sorption analysis** was carried out with a BELSORP mini II (BEL, Japan), applying $N_2$ as adsorbate. Specific surface area was determined using Brunauer-Emmett-Teller (BET) theory, pore analysis was performed using Barrett-Joyner-Halenda (BJH) method and t-plot method respectively.

**Gravimetric $CO_2$ and $N_2$ sorption analysis** were carried out with an IsoSORP Static magnetic suspension balance (Rubotherm) that can be operated up to 200 bar. The significance of the balance was ≤0.1 mg. Thus, a stainless steel sample holder was filled with the $Mg_3N_2$ powder sample and placed at the balance coupling under inert gas flow in order to prevent contact with air and moisture. Subsequently, the balance was evacuated for 6 h at 333 K and $10^{-3}$ mbar until constant mass was achieved. Afterwards, the gas was dosed into the balance chamber to elevated pressures. Equilibrium was achieved within 30 min to 2 h and identified by constant weight and pressure. The temperature was kept constant with an accuracy of ±0.5 K for each measurement. Additionally, a helium buoyancy correction was used to calculate the surface excess mass from the measured values. A detailed description of this procedure can be found elsewhere.[1]

**Optical spectroscopy (UV-Vis spectroscopy)** was recorded with a Varian Cary Scan 100. $Mg_3N_2$ powder samples were pestled with dry $BaSO_4$ under argon and measured in reflectance using an Ulbricht sphere and $BaSO_4$ as reflectance standard.

**Photoluminescence (PL) spectroscopy** was recorded with a Horiba Jobin Yvon Spex Fluorolog 3 (Horiba Jobin Yvon, France) equipped with a 450 W Xe-lamp and double grating excitation and emission monochromator. The determination of the quantum yield was performed according to Friend.[1] First of all, the diffuse reflection of the sample was determined under excitation conditions (maximum of absorption at $\lambda_{exc}$ = 363 nm). Thereafter, the emission was measured at this excitation wavelength. Integration over the reflected and emitted photons by use of the Ulbricht sphere results in the absolute quantum yield. All measurements were referenced to an empty cuvette. Corrections were made regarding the spectral power of the excitation source, the reflection behavior of the Ulbricht sphere, and sensitivity of the detector. To this concern, the FluorEssence Software Version 3.5.8.63 from Horiba Yvon Jobin GmbH was used.

**Fluorescence lifetimes** were obtained as process decay times with the above described Horiba Jobin Yvon Spex Fluorolog 3 spectrometer. The samples were deposited in quartz glass cuvettes under inert-gas atmosphere. The decay times were recorded by time-correlated single-photon counting (TCSPC) with a 370 nm pulsed laser diode. The fluorescence emission was collected at right angles to the excitation source, and the emission wavelength was selected with a monochromator and detected by a photomultiplier as detector. The resulting intensity decays were calculated through tail fit analysis. The quality of the fits was evidenced by low $\chi^2$ values ($\chi^2 < 1.4$).

**2. Characterization of as-prepared, amorphous intermediate**

Subsequent to the ammonolysis of $MgBu_2$ in liquid-crystalline phases with *lq*-$NH_3$, first of all, a colorless and jelly-like intermediate was formed. This amorphous intermediate was characterized by elemental analysis (Table S1), FT-IR spectroscopy (Figure S2), and thermogravimetry (Figure S3).

Elemental analysis (C,H,N analysis) results in a composition $Mg_{1.0}N_{1.5}H_{6.3}C_{1.5}$ with the assumption that the remaining weight relates to magnesium (Table S1). This assumption is reliable since electron energy loss spectroscopy (EELS) points to the absence of oxygen (except for oxygen stemming from the specimen; Figure S1, *see main paper: Figure 5*). Based on FT-IR spectra of the amorphous intermediate (Figure S2), the carbon content as well as significant amounts of hydrogen can be related to heptane as the solvent, which was not completely removed upon drying and which can be assumed to reside inside the pores of the magnesium nitride network. After subtracting the carbon and hydrogen content related to heptane (i.e. $C_{1.5}H_{3.4}$ in regard of the solvent composition $C_7H_{16}$), the stoichiometry of $Mg_{1.0}N_{1.5}H_{2.9}$ with a N : H ratio of 1 : 2 (within the error of the experiment) points to the presence of magnesium amide ($Mg(NH_2)_2$) as the intermediate.

**Table S1.** Elemental analysis (C,H,N) of the amorphous intermediate.

| **Element** | **wt-%** | **atom-%** |
|---|---|---|
| C | 25.2 | 14.2 |
| H | 9.0 | 61.1 |
| N | 30.8 | 14.9 |
| Mg (remain) | 35.0 | 9.8 |

FT-IR spectroscopy confirms the presence of $Mg(NH_2)_2$ and shows the expected characteristic vibrations of magnesium amide with $\nu_{as}$(N–H) at 3341 $cm^{-1}$, $\nu_s$(N–H) at 3277 $cm^{-1}$; $\delta(NH_2)$ at 1572 $cm^{-1}$ as well as lattice vibrations at 685, 650 and 515 $cm^{-1}$ (Figure S2).[2] In addition to vibrations

related to $Mg(NH_2)_2$, vibrations of heptane are observed ($\nu$(C–H): 3000-2750 $cm^{-1}$, finger print area: 1500-900 $cm^{-1}$). Furthermore, a weak vibration at 810 $cm^{-1}$ points to the presence of magnesium imide, Mg(NH), and indicates proceeding ammonolysis from the amide to the imide even at the low temperature of the liquid-$NH_3$-based synthesis (Figure S2). The beginning formation of Mg(NH) also explains the comparably high magnesium content derived from elemental analysis (Table S1: Mg : N = 1.0 : 1.5). In this regard, the Mg : N ratios for $Mg(NH_2)_2$ (1.0 : 2.0) and Mg(NH) (1.0 : 1.0) need to be taken into account.

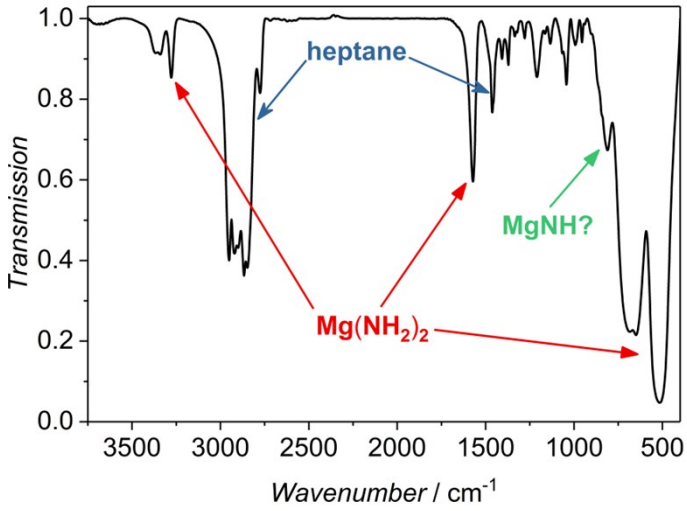


**Figure S2.** FT-IR spectrum of the amorphous intermediate.

Finally, the thermal decomposition of the amorphous intermediate was studied based on thermogravimetry with coupled FT-IR spectroscopy. On the one hand, this allows determining the temperature-dependent release of gases with thermogravimetry. On the other hand, the released gases can be identified via infrared spectroscopy. All these experiments were performed with flowing nitrogen as atmosphere. Accordingly, the thermal decomposition of the amorphous intermediate shows four overlapping decomposition steps at 50-150, 150-290, 290-395, and 395-500 °C with a total weight loss of 48.3% (Table S2, Figure S3a).

In combination with FT-IR spectroscopy, the gaseous decomposition products of the first and the second decomposition step can be reliably identified as heptane predominately showing characteristic $\nu$(C–H) vibrations (3000-2750 $cm^{-1}$) (Table S2, Figure S3a-c). Both decomposition steps at higher temperature can be related to the release of $NH_3$ ($\nu$(N–H): 3294 $cm^{-1}$, $\delta(NH_3)$: 1628, 957, 931 $cm^{-1}$) upon formation of magnesium imide (Mg(NH)) in step 3 and the completion of the ammonolysis with formation of $Mg_3N_2$ in step 4 (Table S2, Figure S3a-c). Taking the specific sample weight prior to the $NH_3$ release as 100%, the release of $NH_3$ relates to 26% in step 3, and 10% in step 4, which is well in accordance with the values calculated via the following reactions:

Step 3: $Mg(NH_2)_2 \rightarrow Mg(NH) + NH_3$ (calculated release: 28%)

Step 4: $3Mg(NH) \rightarrow Mg_3N_2 + NH_3$ (calculated release: 13%)

**Table S2.** Release of gases upon thermal decomposition of the amorphous intermediate according to FT-IR-coupled thermogravimetry (Figure S3).

| **Decomposition temperature / °C** | **Release of gases wt-%** | **Type of gas (according to FT-IR coupling)** |
|---|---|---|
| 1. 50-150 | 7.4 | Heptane |
| 2. 150-290 | 15.6 | Heptane |
| 3. 290-395 | 19.6 | $NH_3$ |
| 4. 395-500 | 5.8 | $NH_3$ |

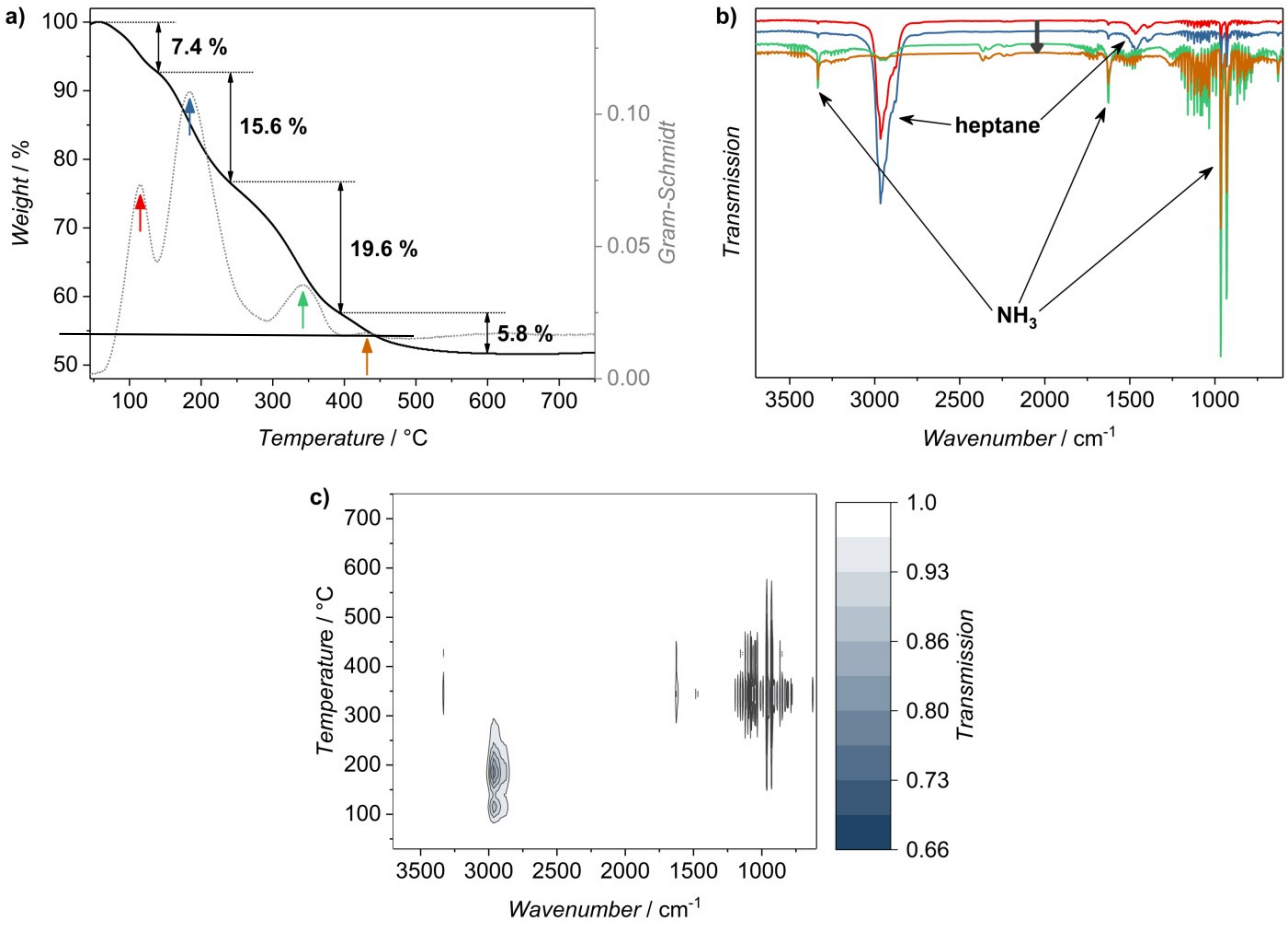


**Figure S3.** FT-IR-coupled thermogravimetry (TG) of the amorphous intermediate as observed in $N_2$ gas flow: a) TG analysis with respective Gram-Schmidt curve; b) FT-IR spectra of the released gas at specific temperatures of decomposition (115, 182, 341, 431 °C) indicated by colored arrows in the Gram-Schmidt curve (a); c) Two-dimensional illustration of temperature-dependent FT-IR spectra.

Again, these results point to $Mg(NH_2)_2$ as chemical composition of the amorphous intermediate obtained directly after *lq*-$NH_3$-based reaction and prior to thermal annealing. Taking all decomposition steps into account – including heptane and $NH_3$ – TG is also well in agreement with the sum composition $Mg_{1.0}N_{1.5}H_{6.3}C_{1.5}$ obtained via elemental analysis (Table S1). Thus, the calculated total weight loss related to this sum formula with 51.7% is well in agreement with the total weight loss obtained from TG (48.3%, Table S2, Figure S3a). Finally, it must be noted that the here observed thermal decomposition is in good agreement with comparable experimental data reported by *Dolci et al.* for bulk magnesium amide.[3] They could also identify the composition and structure of the intermediate products via neutron scattering.

### 3. Luminescence characterization

In addition to luminescence characterization after annealing at 600 °C (*see main paper: Figure S9*), we also performed the luminescence characterization after annealing at 800 °C (Figure S4). With this measure, we intended to reduce the defect level and to improve crystallinity. As a result, we found that annealing $Mg_3N_2$ at 600 °C is optimal in regard of the luminescence properties including emission intensity and quantum yield. These findings can be explained by the larger surface area and the higher concentration of surface-related defects upon annealing at 500 °C resulting in a higher level of defect-related loss processes. Increasing the annealing temperature from 600 to 800 °C, however, also leads to a lower emission intensity and quantum yield (15-20%) due to beginning thermal decomposition of $Mg_3N_2$.

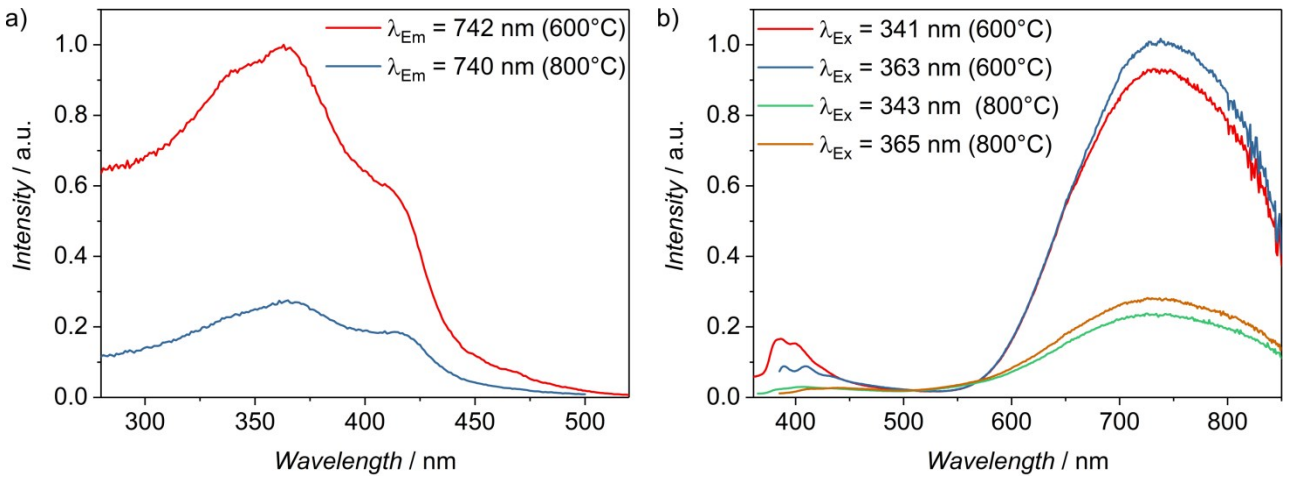


**Figure S4.** Comparison of excitation (a) and emission (b) spectra of $Mg_3N_2$ annealed at 600 and 800 °C.

Fluorescence lifetimes of $Mg_3N_2$ (annealed at 600 °C) were measured upon excitation with a 370 nm pulsed laser diode and monitored for the emissions at 399 and 742 nm (Figure S5). An

empty cuvette was used as a reference. Both the $Mg_3N_2$ sample and the empty cuvette show a more-or-less identical decay in the 0.1 ns regime (Figure S5). In fact, this decay relates to the limit of the time resolution of the applied 370 nm pulsed laser diode. Thus, the fluorescence decay of the high-porosity $Mg_3N_2$ occurs on an even shorter time scale (<0.1 ns). This finding clearly points to fluorescence behaviour with quantum-mechanically allowed transitions. Such fluorescence lifetimes are expected for semiconductors without specific donor-acceptor doping and were similarly reported, for instance, for zinc oxide.[4]

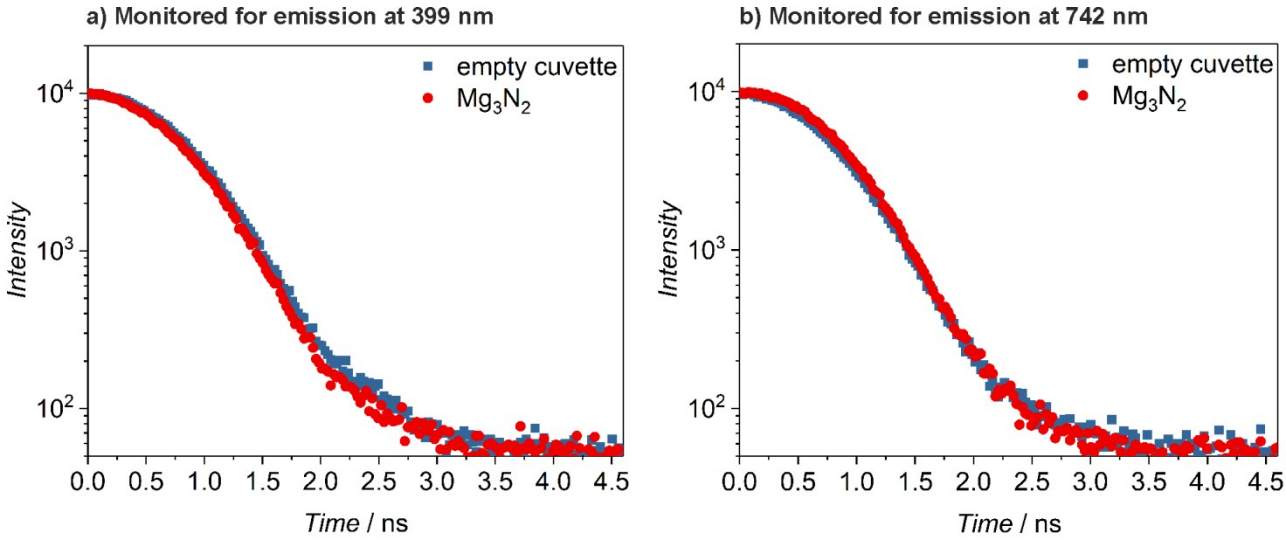


**Figure S5.** Fluorescence lifetimes of $Mg_3N_2$ (annealed at 600 °C) monitored for the emissions at 399 and 742 nm with empty cuvette as a reference.

## References


1 J. V. de Mello, H. F. Wittmann and R. H. Friend, *Adv. Mater.*, 1997, **9**, 230.

2 G. Linde and R. Juza, *Z. Anorg. Allg. Chem.*, 1974, **409**, 199.

3 F. Dolci, E. Napolitano, E. Weidner, S. Enzo, P. Moretto, M. Brunelli, T. Hansen, M. Fichtner and W. Lohstroh, *Inorg. Chem.*, 2011, **50**, 1116.

4 Reviews: a) P. A. Rodnyi and I. V. Khodyuk, *Optics and Spectroscopy*, 2011, **111**, 776. b) B. K. Meyer, H. Alves, D. M. Hofmann, W. Kriegseis, D. Forster, F. Bertram, J. Christen, A. Hoffmann, M. Straßburg, M. Dworzak, U. Haboeck and A. V. Rodina, Phys. Stat. Sol. B, 2004, **241**, 231.